Resource

Cell Reports

Peptide-Based Scaffolds Support Human Cortical Progenitor Graft Integration to Reduce Atrophy and Promote Functional Repair in a Model of Stroke

Graphical Abstract

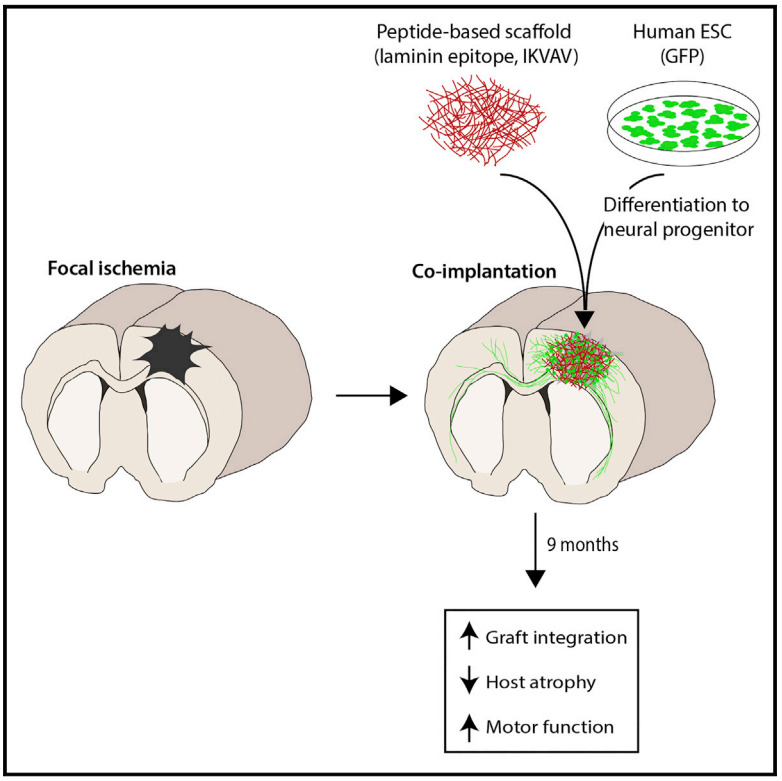

Highlights

- Peptide scaffolds structurally and functionally support neural grafts in a stroke model
- Scaffolds promote human stem cell graft differentiation and integration
- Cell + scaffold implants reduce host tissue atrophy
- Cell + scaffold implants promote prolonged recovery of motor function

Authors

Fahad A. Somaa, Ting-Yi Wang, Jonathan C. Niclis, ..., David R. Nisbet, Lachlan H. Thompson, Clare L. Parish

Correspondence

lachlan.thompson@florey.edu.au (L.H.T.), clare.parish@florey.edu.au (C.L.P.)

In Brief

Somaa et al. examine the capacity of peptide-based scaffolds to structurally and functionally support human pluripotent stem cell-derived neural transplants in the stroke-injured brain. Scaffolds promoted graft maturation and integration and reduced host tissue atrophy, resulting in improved motor function over a period of 9 months.

Somaa et al., 2017, Cell Reports *20*, 1964–1977
August 22, 2017
http://dx.doi.org/10.1016/j.celrep.2017.07.069

CellPress

OPEN ACCESS
CellPress

Cell Reports
Resource

Peptide-Based Scaffolds Support Human Cortical Progenitor Graft Integration to Reduce Atrophy and Promote Functional Repair in a Model of Stroke

Fahad A. Somaa,[1,4] Ting-Yi Wang,[1,4] Jonathan C. Niclis,[1,4] Kiara F. Bruggeman,[2] Jessica A. Kauhausen,[1] Haoyao Guo,[1] Stuart McDougall,[1] Richard J. Williams,[3] David R. Nisbet,[2] Lachlan H. Thompson,[1,5,*] and Clare L. Parish[1,5,6,*]
[1]The Florey Institute of Neuroscience and Mental Health, The University of Melbourne, Parkville, VIC 3052, Australia
[2]Laboratory of Advanced Materials, Research School of Engineering, The Australian National University, Canberra, ACT 2601, Australia
[3]School of Engineering, RMIT University, Melbourne, VIC 3001, Australia
[4]These authors contributed equally
[5]Senior author
[6]Lead Contact
*Correspondence: lachlan.thompson@florey.edu.au (L.H.T.), clare.parish@florey.edu.au (C.L.P.)
http://dx.doi.org/10.1016/j.celrep.2017.07.069

SUMMARY

Stem cell transplants offer significant hope for brain repair following ischemic damage. Pre-clinical work suggests that therapeutic mechanisms may be multi-faceted, incorporating bone-fide circuit reconstruction by transplanted neurons, but also protection/regeneration of host circuitry. Here, we engineered hydrogel scaffolds to form "bio-bridges" within the necrotic lesion cavity, providing physical and trophic support to transplanted human embryonic stem cell-derived cortical progenitors, as well as residual host neurons. Scaffolds were fabricated by the self-assembly of peptides for a laminin-derived epitope (IKVAV), thereby mimicking the brain's major extracellular protein. Following focal ischemia in rats, scaffold-supported cell transplants induced progressive motor improvements over 9 months, compared to cell- or scaffold-only implants. These grafts were larger, exhibited greater neuronal differentiation, and showed enhanced electrophysiological properties reflective of mature, integrated neurons. Varying graft timing post-injury enabled us to attribute repair to both neuroprotection and circuit replacement. These findings highlight strategies to improve the efficiency of stem cell grafts for brain repair.

INTRODUCTION

Loss of neurons in the cerebral cortex underlies much of the motor, sensory, and cognitive dysfunction in stroke patients, with disability due to primary neuronal loss, as well as additional ongoing secondary degeneration in the surrounding penumbra (Lindvall and Kokaia, 2011). With the exception of surgical clot removal or thrombolytic drugs, both targeted at restoring perfusion and penumbral protection, no effective treatment is currently available to improve functional recovery in patients (Lindvall and Kokaia, 2011). Circuit replacement, through transplantation of neural progenitor cells (NPCs) generated from pluripotent stem cells (PSCs), represents a hopeful and realistic therapeutic strategy.

Clinical proof-of-principle for this approach is drawn from Parkinson's disease patient trials where transplanted dopamine neurons reinnervate the denervated striatum, resulting in sustained improvement of motor function (Barker et al., 2013). A fundamental requirement for therapeutic efficacy is the correct specification of transplanted neurons in order to facilitate functional innervation of appropriate targets (Thompson and Björklund, 2012).

For acute brain injuries, including ischemic stroke, the requirement for functional connectivity is less clear. Pre-clinical studies have demonstrated therapeutic benefits associated with transplant-mediated effects on host tissue including penumbral protection, enhanced angiogenesis, modulation of inflammation, and stimulation of compensatory plasticity (Lindvall and Kokaia, 2011). This has stimulated interest in the use of non-neural cells, such as mesenchymal stem cells, as donor-cell preparations aimed squarely at conferring benefit through these homeostatic mechanisms (Cao and Li, 2015). While promising, functional recovery is often incomplete and may be limited by extensive non-recoverable damage. Thus, additional functional recovery through bona-fide circuit reconstruction remains a promising strategy.

PSCs hold significant potential as a donor source for cell replacement in stroke. Routine procedures now exist for generating a diverse range of neuronal subtypes, including specification into cortical projection neurons (Shi et al., 2012; Chambers et al., 2009) relevant for replacement of cortical circuitry damaged after stroke. Following transplantation, PSC-derived neurons exhibit a remarkable capacity for long-range anatomical integration and development of appropriate electrophysiological properties (Denham et al., 2012; Espuny-Camacho et al., 2013; Niclis et al., 2017b; Steinbeck et al., 2012). In rodent models of stroke, various degrees of functional recovery have been reported (Daadi et al., 2008; Gomi et al., 2012; Jensen et al., 2013; Jiang et al., 2011; Oki et al., 2012; Qin et al., 2013; Tatarishvili et al., 2014; Tornero et al., 2013), but over time frames inconsistent with functional maturity of implanted neurons.

Thus, direct contribution to functional neuronal replacement has been difficult to assess.

Long-term survival and integration of grafted neurons may be particularly challenging in a stroke-affected hostile environment characterized by a cystic cavity, highly vulnerable peri-infarct tissue, and proinflammatory cues (Jendelová et al., 2016). Use of biomaterials is increasingly being recognized as a valuable adjunct approach for cell-based therapies and may impart physical and trophic support to both host and grafted cells (Jendelová et al., 2016). A variety of natural and synthetic polymers, such as collagen, chitosan, and poly(lactic acid), as well as decellularized scaffolds, have been employed to support neural grafts in the ischemic brain (Bible et al., 2009, 2012; Cheng et al., 2013; Elias and Spector, 2012; Jin et al., 2010; Liang et al., 2013; Park et al., 2002; Yu et al., 2010; Zhong et al., 2010). While these materials have shown variable anatomical and functional benefits, most optimal for regenerative medicine will be the employment of readily injectable nanomaterials that self-assemble from biologically active molecules. Few studies have examined the potential for synthetic, but biomimetic, self-assembling peptide (SAP) scaffolds with transplantation and have focused on endogenous neuron survival and plasticity (Ellis-Behnke et al., 2006; Guo et al., 2009). Here, we report the use of an injectable biological substrate that facilitates long-term survival and functional maturation of human PSC (hPSC)-derived cortical neurons, when implanted into the site of cortical ischemic. We report this functionalized scaffold restored tissue architecture within the lesion cavity, reduced atrophy and cell loss within the penumbra, while additionally supported cortical neuronal differentiation of human PSC grafts. Scaffold-supported transplants were capable of prolonged restoration of motor function, providing evidence of sustained benefits of human stem cells and biomaterials in repair of the ischemic brain.

RESULTS

Characterization of Peptide-Based Scaffolds and Stem Cell Differentiation

To rebuild the local architecture at the primary injury site and support the integration of grafts into the surrounding host tissue, we tailored a biomaterial to provide structural scaffolding and biomimetic of the brain's extracellular matrix. The synthesized scaffold incorporated the laminin binding domain peptide sequence, IKVAV, necessary for neural adhesion, migration, differentiation, and axonal plasticity (Matson et al., 2011). SAPs were optimized for assembly at pH 7.4, by adjustment of the pKa, through the addition of two aspartate residues, giving the resultant peptide sequence DDIKVAV (Figure 1A). Aromatic fluorenylmethyloxycarbonyl (Fmoc) moieties were used to protect the amino terminus of the peptide and provide shared electrons to form π-π interactions, creating a backbone structure (Figures 1A and 1B, red). The individual peptides interacted via hydrogen bonds to form secondary protein β sheets (Figure 1C), confirmed by spectroscopic analysis (Figures 1F and 1G). Through a combination of amphiphilic organization, π-π interactions, and β sheets, nanotubes were formed (Figure 1D) that interacted to create highly hydrated bundles and provided the underlying matrix (Figure 1E). Nanofibrous structure was confirmed via electron microscopy (Figure 1H), while rheological analysis validated viscoelastic gel properties, demonstrating that the resultant hydrogel had a modulus not dissimilar to the rat brain (Figure 1I) and was thereby suitable for brain repair.

Cortical progenitors were generated via dual SMAD inhibition of hPSCs, resulting in neural induction and dorsal forebrain specification, as shown by the presence of rosettes and neural-ridge structures at 10 days in vitro (DIV) and expression of the NPC marker SOX2, dorsal telencephalic marker PAX6, and forebrain/midbrain transcription factor OTX2 (Figures 1J and 1K). These forebrain progenitors, expanded as neurospheres, showed maintained GFP, OTX2, and Nestin expression at the time of transplantation (Figures 1L and 1M, 17 DIV).

SAP-Supported Neural Grafts Improve Sensorimotor Function in Ischemic Rats

Staircase testing of fine and coordinated forelimb sensorimotor function was performed in rats receiving unilateral intracortical ischemic insults and cell ± SAP implants at 3 weeks (Figure 2A). ET1-lesioned rats showed a reduced proportion of pellets eaten with the impaired (left) paw, compared to saline-injected controls (Figure 2A, intact, white triangles), prior to grafting, a deficit that remained persistent and stable for 36 weeks (Figure 2A, gray triangles). Limb use was significantly improved in ET1 rats receiving cell implants (ET1 + cells: 33.8 ± 2.4%; Figure 2A, gray circles) at 36 weeks compared to controls (ET1: 22.4 ± 2.3%) and notably more rapid in animals grafted with cells and scaffolds (ET1 + cells+SAP), with significant improvements observed as early as 16 weeks (33.9 ± 2.4%; Figure 2A, black circles). By 36 weeks cells+SAP implants continued to provide a significant benefit (41.3 ± 1.3%), with limb function not different from intact controls (41.7 ± 2.9%) and significantly greater than observed for cells alone. Note that SAP implants, in the absence of cells, provided no significant benefit for forelimb function, (26.0 + 3.1%; Figure 2A, white circles).

Prior to killing animals for histology, additional motor function tests were performed. The rotarod test, a measure of balance, coordination, and physical condition (particularly of the hindlimbs), revealed no gross motor impairment resulting from ischemia at 36 weeks (Figure 2B). In the cylinder test, a measure of bias in limb use, ET1 and ET1 + SAP-implanted animals showed a significant impairment in contralateral forelimb use, reflected by reduced weight-bearing left forepaw touches on the cylinder wall, compared to saline-injected controls (Figure 2C). Only ischemic animals receiving cells+SAP grafts showed a significant improvement in left paw use compared to ET1-lesioned rats (52.1 ± 5.5% and 26.5 ± 4.7% wall touches using left paw, respectively), function that was not statistically separable from intact controls (51.8 ± 2.5%). The adjusted stepping test highlighted forelimb akinesia in ET1-lesioned animals, as revealed by significant reductions in left paw forehand and backhand touches at 36 weeks, that was partially restored only in animals receiving cells+SAP transplants (Figures 2D and 2E).

SAP Scaffolds Provide Structural and Biochemical Support for Transplanted Cortical Progenitors in the Ischemic Brain

At 36 weeks after receiving implants into the ischemic cortex, the majority of animals were taken for histological analysis. Human

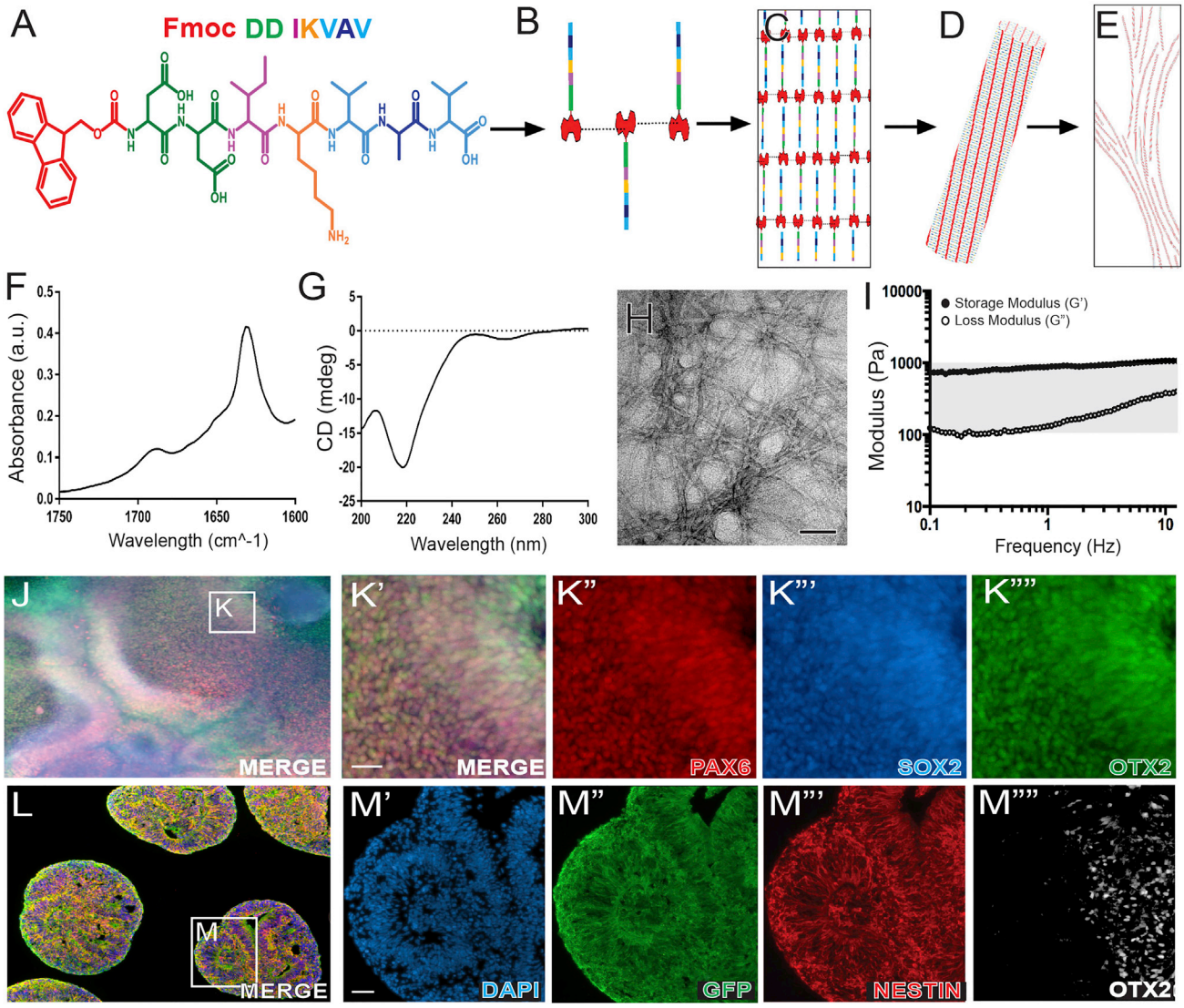

Figure 1. Generation of DDIKVAV SAP Scaffolds and hESC-Derived Cortical Progenitors Suitable for Transplantation

(A) Chemical structure of Fmoc-DDIKVAV synthesized via solid-phase peptide synthesis.

(B–E) Schematic of Fmoc-self-assembly process.

(B) Aromatic Fmoc terminal groups undergo π stacking.

(C) The DDIKVAV peptide chains undergo hydrogen bonding to form β sheets.

(D) A natural twist occurs to maintain this π-β assembly, forming a hollow nanofiber with the DDIKVAV sequence exposed on the outside of the fiber.

(E) The nanofibers interact with each other forming a nanofibrous network.

(F and G) FTIR analysis of amide I region (F) showed characteristic peak for β sheets with an observable carbamate peak, and the stable formation of a dominant assembly confirmed by (G) circular dichroism spectroscopy, showing transition peak at 220 nm.

(H) Electron microscopic image of the Fmoc-DDIKVAV gel showing nanofibers. Scale bar, 100 nm.

(I) Rheological frequency measurements of the elastic shear moduli of storage (G', black dots) and loss modulus (G," white dots). The grey area represents the modulus of the rat brain.

(J) Low-magnification photomicrographs of hESCs differentiated as adherent cultures under dual SMAD conditions.

(K) Inset taken from (J); high-magnification images (K'–K'''') illustrating that differentiation resulted in the formation of neural rosettes and ridges that were immunoreactive for dorsal forebrain markers PAX6 (K"), SOX2 (K"'), and OTX2 (K"") by 10 DIV.

(L and M) Cultures were subsequently expanded and matured in suspension as floating neurospheres (L), with DAPI-labeled cells (M') immunoreactive for GFP (M") and widely co-expressing NESTIN (M"') and OTX2 (M"").

Scale bars, 100 nm (H) and 50 μm (K and M).

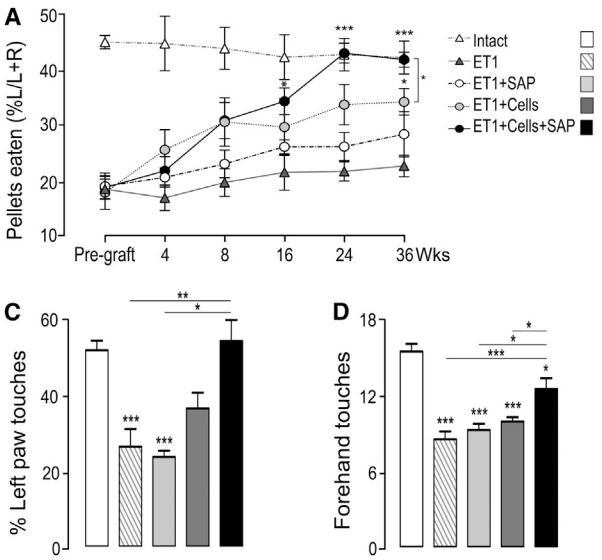

Figure 2. Transplantation of hESC-Derived Progenitors, in the Presence of SAP Scaffolds, Improves Motor Function in Ischemic Rats

(A–E) Comparative performance in rotarod (A), staircase (B), cylinder (C), and adjusted stepping (D and E) tests of control rats (intact, n = 12), and rats subjected to unilateral ET1 lesion of the right sensorimotor cortex (ET1, n = 20), followed by implants at 3 weeks of SAP scaffolds (ET1 + SAP, n = 8), hESC-derived cortical progenitor cells (ET1 + cells, n = 12), or cell + SAP scaffold (n = 13).

(A) Time course of staircase performance in ET1 rats revealed significant improvements in pellet retrievals using the impaired left paw by 16 weeks in animals receiving cells+SAP implants, not observable until 36 weeks in rats grafted with cells alone, and absent in animals receiving SAP-only implants.

(B) No gross motor deficits were observed in any ET1-lesioned animals (±cell/SAP implants) after 36 weeks, with animals displaying the ability to remain on the rotating rod.

(C) Performance in the cylinder test revealed a persistent functional deficit in the impaired paw (% left paw touches/total touches) in ET1 and ET1 + SAP animals at 36 weeks, that was significantly corrected in cell and cells+SAP-grafted rats.

(D and E) Performance in the stepping test, presented as number of touches with forehand (D) and backhand (E) of the left forelimb, revealed significant improvements in limb function only in animals receiving cells+SAP transplants.

embryonic stem cell (hESC)-derived cortical progenitor grafts, in the absence or presence of SAP, could be identified within the host cortex of ischemic rats by GFP labeling (Figures 3A and 3B). Volumetric and stereological analysis of the delineated GFP^+ grafts (implanted 3 weeks after ET1 administration) revealed that grafts in the presence of SAP scaffolds were notably larger (cells: 3.5 ± 1.8 mm^3 and cells+SAP: 10.7 ± 3.8 mm^3; Figures 3A–3C), correspondingly contained more $DAPI^+$ cells (cells: $8.5 \times 10^5 \pm 3.6 \times 10^5$ and cells+SAP: $30.5 \times 10^5 \pm 7.5 \times 10^5$; Figure 3D), and thereby maintained a cellular density similar to cell-only transplants, yet were visibly greater in density than the host cortex (Figures 3E–3G).

To characterize morphological properties of grafts, examination of neural markers together with GFP immunoreactivity was performed. Reflective of the ability of grafted cells to integrate into the host tissue, and not be impeded by either the scaffold or host scar tissue, numerous doublecortin migrating neuroblasts (DCN^+GFP^+) were observed at the edge of the grafts and within the surrounding host parenchyma (Figure 3K). Both cells and cells+SAP grafts contained all neural lineages including mature neurons ($NEUN^+GFP^+$; Figure 3L), astrocytes (glial fibrillary acidic protein $[GFAP]^+GFP^+$; Figure 3L), and oligodendrocytes ($OLIG2^+GFP^+$, RIP^+GFP^+; Figure 3M). Cell grafts were notably heterogeneous, containing dense patches of $NEUN^+$ cells adjacent to regions almost devoid of neurons, resulting in a neuronal density of 49.7% ± 8.8%. Comparatively, cell + SAP grafts were more differentiated and homogeneous with 69.6% ± 2.9% $NEUN^+/GFP^+DAPI^+$ (Figures 3H, 3N, and 3O). We also assessed grafts for the presence of cortical layer selective neuronal populations including the T box transcription factor, TBR1 (deep layers V–VI) and POU homeodomain protein, BRN2 (superficial layers II–IV) (Shi et al., 2012). As a proportion of total neurons, cell grafts contained 37.6 ± 11.2% BRN2 and 7.4 ± 1.1% TBR1 neurons, while cells+SAP grafts contained a significant increase in the proportion of both BRN2 (65.8 ± 4.4%) and TBR1 (20.0 ± 2.7%) neurons (Figures 3I, 3J, and 3P–3S), suggesting the SAP scaffold impacted on the neuronal differentiation and phenotype acquisition of the progenitors in situ. Furthermore, in both cell and cells+SAP grafts, a dense network of vesicular glutamate transporter ($VGLUT^+$) glutamatergic fiber innervation could be observed (Figure 3T). Other neuronal populations were relatively sparse or absent, including γ-aminobutyric acid (GABA) (Figure 3T), tyrosine hydroxylase (TH), 5HT, and choline acetyltransferase (ChAT) (data not shown). Interestingly, motor performance in the staircase test at 36 weeks correlated with graft volume, total cells within the graft (GFP^+DAPI^+), and proportion of neurons (including cortical subpopulations), with those animals receiving cells+SAP implants (3 weeks after ET1 administration) displaying the greatest functional improvement and largest grafts with greatest neuronal proportions (Figure S2) (related to Figures 2 and 3).

Graft integration was assessed at 36 weeks after implantation by the presence and density of GFP^+ fibers with the surrounding host parenchyma. No discernable difference was observed in the pattern of axonal growth between cells and cells+SAP-implanted animals, with GFP^+ axonal projections observed emanating from the graft and extending long distances both rostro-caudally and dorso-ventrally from the site of implantation (Figure 4). Large bundles of GFP^+ axons grew along the host white matter of the corpus callosum (Figure 4Ci) to innervate both the ipsi- and contralateral hemispheres. GFP^+ fibers could be observed as rostral as the olfactory bulb (data not show) and shell of the nucleus accumbens (Figures 4A and 4Ai) and as caudal as the midbrain (Figures 4D and 4Di). Innervation was most prominent within the motor, somatosensory, cingulate, piriform, and entorhinal cortex (Figures 4Bi–4Biv), reflective of

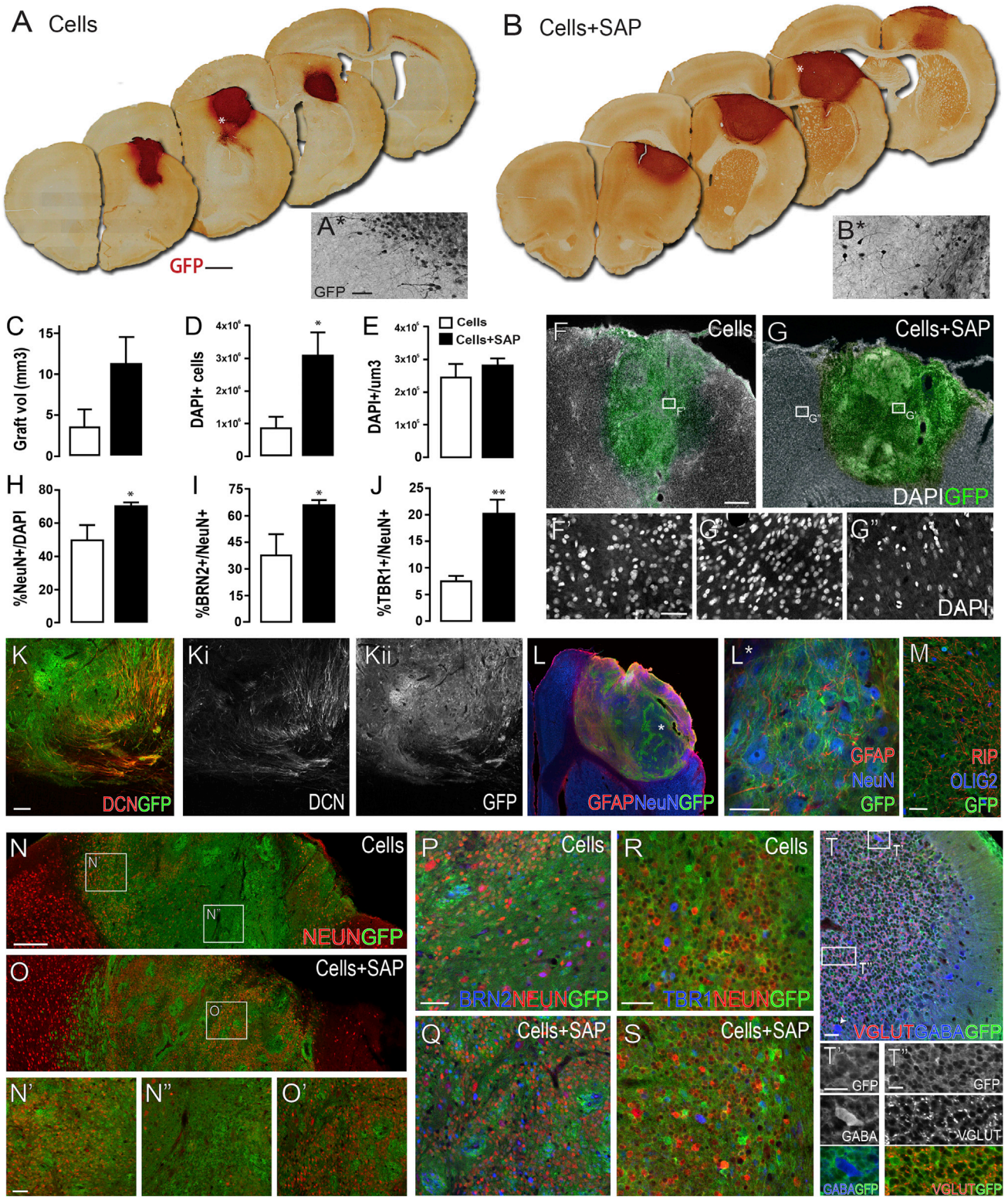

Figure 3. SAP Scaffolds Support hESC-Derived Progenitor Grafts and Their Cortical Neuronal Specification

(A and B) Representative photomicrographs providing a coronal projected view of a GFP-expressing human ESC-derived cortical progenitor graft, implanted at 3 weeks after ET1 administration and assessed 36 weeks later, in the absence (cells, A) and presence of an IKVAV SAP scaffolds (cells+SAP, B). (A* and B*) High power micrographs illustrating the morphology of GFP-labeled cells at the edge of the graft.

(legend continued on next page)

layers II–V cortical projection neurons. Networks of GFP$^+$ fibers were also observed in subcortical nuclei, including the hippocampus, lateral septum, striatum (Figures 4E, 4Bv, and 4Bvi), and more sparsely in the ventral thalamus and hypothalamus (Figures 4Cii and 4Ciii). Densitometric analysis of GFP-labeled fibers in the motor cortex adjacent to the graft, and at distal cortical target sites (ipsi- and contralateral entorhinal cortex), confirmed the similarity in innervation density between cell and cell + SAP grafts (Figure 4F).

Cortical Progenitor Grafts Are Highly Vascularized and Show No Evidence of Neural Overgrowth 9 Months after Transplantation

Necessary for the survival of transplanted neurons is their close association to a vascular supply, with reports of neurons surviving poorly at distances greater than 75 μm from the nearest blood vessel (Casper et al., 2003). In light of the large size of the hESC-derived cortical progenitor grafts observed, we examined the extent to which the new tissue was vascularized. RECA-1 immunostaining revealed a dense network of blood vessels in both cells and cells+SAP grafts (Figures 5A and 5B) that was not dissimilar between the two graft groups. Vessels within grafts were significantly hypertrophied compared to the host cortex (vessel diameter, host cortex: 18.6 ± 0.4 μm, cells graft: 35.5 ± 1.7 μm, cells ± SAP graft: 36.5 + 0.6 μm), lower in density (area covered by RECA1$^+$ in the host cortex: 25.4 ± 0.8%; cell graft: 14.5 ± 1.5% and cells+SAP graft: 13.9 ± 0.7%; Figure 5C), and likely reflect immature vessel formation and/or a feature of vascularization of human verse rodent tissue.

Closer examination revealed that RECA1$^+$ vessels within the grafts were GFP$^-$ (Figure 5D') and thus host-derived. In addition, we observed extensive RECA1$^+$ staining of vessels within the host tissue surrounding the graft (32.3 ± 0.4%), significantly greater than in the cortex of unlesioned animals, and indicative of important revascularization of the penumbra (Figures 5B'' and 5C).

While hESCs were pre-differentiated in vitro and showed high neural composition within the grafts (including cortical identity) at 9 months, we importantly observed no gross morphological features within the grafts suggestive of excessive cell division or tumors. At 9 months, less than 0.5% of cells were dividing (Figures 5E–5G, %Ki67/DAPI), with only occasional small Ki67$^+$ clusters observed within the grafts, that were often GFP$^-$ and localized around RECA1$^+$ vessels (Figure 5D''), indicative of host involvement in vascularization of the new tissue.

A challenge working with athymic nude rats over extended periods of time, particularly where excessive handling is involved (such as for repeat surgeries and behavioral testing) is their susceptibility to pathogens. Consequently, during the course of the study a small number of animals were euthanized prior to 36 weeks due to unrelated skin and intestinal-related health concerns. These animals provided important insights into the growth kinetics of grafts. Irrespective of graft age, and despite the steady increases in graft volume over time (Figures S3A, related to Figure 5), no OCT4$^+$ cells were observed in any animals (data not shown). Evident within younger grafts, however, was the trend toward an increased proportion of Ki67$^+$ dividing cells within cells+SAP grafts at 5–7 months compared to cells alone (Figure S3B), suggesting that the scaffold may contribute to prolonging proliferation of the neuronal progenitor pool, a role recently attributed to IKVAV signaling (Sahab Negah et al., 2016).

Human ESC-Derived Neurons, Grafted with SAP Scaffolds, Develop Functional Electrophysiological Properties in the Ischemic Cortex

To determine whether grafted cells behaved as functionally connected neurons, brain slices from cells and cells+SAP-implanted animals were taken for eletrophysiological analysis. Native GFP fluorescence allowed for rapid identification of grafted cells (Figure 6Ai) that were patched for whole-cell recordings under Dodt contrast (Figure 6Aii). Interestingly, SAP fibers were visible within the slices, indicating maintained integrity of the SAP scaffold gel at 9 months (Figure 6Aii). Patch-clamped cells were depolarized via current injections to activate voltage-activated channels if present. Various spiking patterns were noted in both cells and cells+SAP-grafted tissue (Figures 6D and 6E), including regular firing, fast spiking (Figure 6Di), and intermittent bursting (Figure 6Dii). Supported by reduced neuronal differentiation seen in cells-only grafts were responses indicative of no voltage-activated channel expression (Figure 6Diii), a feature of immature neurons and astrocytes. For neurons in both graft types, action potential firing patterns were similar across various neuronal types (Figure 6F). Cells exhibited resting membrane potentials as follows: cell-only grafted neurons (−68 ± 2 mV, n = 5), cell-only grafted ''immature neurons/astrocytes'' (−74 ± 2 mV, n = 4), and cells+SAP-grafted neurons (−61 ± 2 mV, n = 7). In voltage clamp, we assessed pre-synaptic connectivity to neurons by recording both spontaneous excitatory and inhibitory post-synaptic currents (Figure 6G). In cell-only grafts, 4/5 recorded cells exhibited excitatory post-synaptic currents

(C–E) The volume of the graft core (C) commensurately increased with DAPI cell numbers (D), resulting in no difference in the density of cells within the graft (E).
(F and G) Representative images showing DAPI density within cells (F) and cells+SAP grafts (G).
(F', G', and G'') Note cell density was not different between cell and cells+SAP grafts (F' and G'), but was notably higher than the host tissue (G'').
(H–J) Quantification of NEUN$^+$/DAPI (H), TBR1$^+$/NEUN$^+$ (I), and BRN2$^+$/NEUN$^+$ cells (J) within the delineated GFP$^+$ grafts revealed increased neuronal maturation and cortical specification of grafted cells in the presence of the scaffold.
(K–T) Numerous GFP$^+$ migrating neuroblasts, expressing doublecortin (DCX), were observed at the graft periphery and infiltrating into the host tissue (K). Cell grafts, in the presence and absence of SAP scaffolds, contained all neural lineages, including NEUN$^+$ neurons and GFAP$^+$ astrocytes (L), as well as OLIG2$^+$, RIP$^+$, and oligodendrocytes (M). Exposure of cell grafts to SAP scaffolds significantly increased the proportion of NEUN$^+$ cells (NEUN$^+$/DAPI$^+$; N and O) and, more specifically, the proportion of deep (BRN2$^+$/NEUN$^+$; P and Q), as well as superficial cortical layer (TBR1$^+$/NEUN$^+$; R and S) neurons, compared to cell-only implants. (T) Reflective of the cortical identity of transplanted neurons, cell grafts (in the presence or absence of the SAP scaffold) were rich in glutamatergic innervation (vGLUT, T''), while other neuronal fates, including GABA (T'), were relatively sparse.
Data represent mean ± SEM, *$p < 0.05$, **$p < 0.01$, and ***$p < 0.001$. Scales bars, 1 mm (A and B), 100 μm (A* and B*), 500 μm (F, G, and M), 50 μm (F', G', G'', K, L, N', N'', O', and T), 25 μm (M', T', and T''), and 200 μm (N and O).

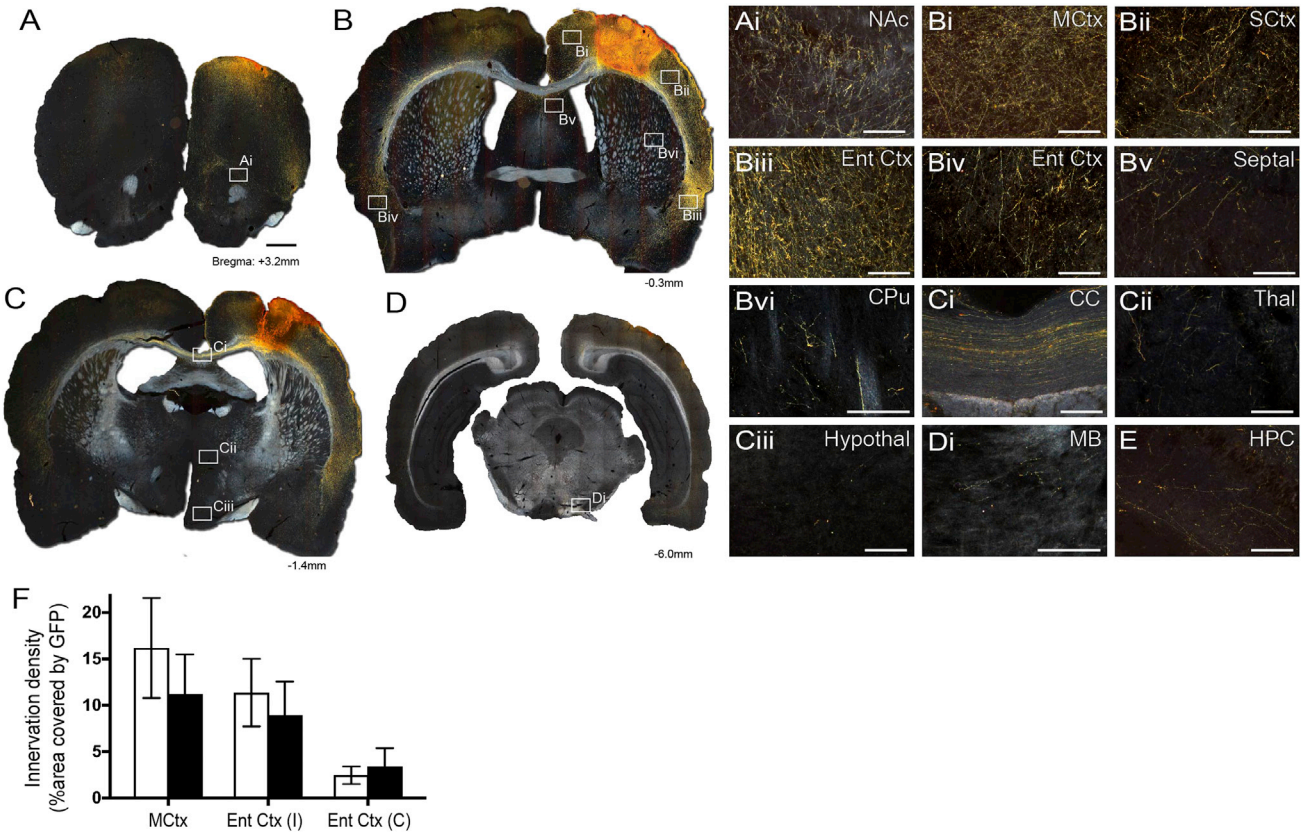

Figure 4. Human ESC-Derived Cortical Progenitor Grafts Display Extensive Axonal Growth along White Matter Tracts and Innervation of Cortical Targets

(A–D) Dark field images illustrating the GFP$^+$ graft and level of extensive axonal growth from the graft into the host brain.

(Ai and D) GFP fibers were observed throughout the rostro-caudal plane reaching targets as far rostral as the olfactory bulb and nucleus accumbens (Ai) and as caudal as the midbrain (D).

(Bi–Biii) GFP fibers were additionally seen throughout the dorso-lateral axis of the brain, with density greatest within the ipsilateral host cortex, including the motor (Bi), sensorimotor (Bii), and cingulate cortex, yet bundles of GFP$^+$ fibers were also observed coursing through forceps minor to innervate ventral cortical nuclei (Biii).

(Biv and Ci) Dense bundles of GFP$^+$ fibers were observed traversing the corpus callosum (Ci) to innervate the contralateral hemisphere, where similar patterns of cortical innervation, albeit fewer in density, were observed (Biv).

(Bv, Bvi, Cii, Ciii, and E) GFP fibers were additionally observed within subcortical nuclei including the lateral septum (Bv), striatum (Bvi), hippocampus (E), thalamus (Cii), hypothalamus (Ciii), and midbrain (Di).

(F) Density of graft-derived GFP$^+$ fibers within the host brain, proximal (MCtx) and distal (Ent Ctx, ipsilateral, I, and contralateral, C) to the site of implantation, revealed no difference in patterns or density of innervation between cells and cells+SAP grafts. Mean ± SEM, Student's t tests. Scale bars, 100 μm.

NAc, nucleus accumbens; MCtx, motor cortex; SCtx, somatosensory cortex; EntCtx, enthorinal cortex; Thal, thalamus; CPu, striatum; CC, corpus callosum; HPC, hippocampus; MB, midbrain; hypothal, hypothalamus. Scale bars, 1 mm (A–D) and 100 μm (higher magnification insets).

(EPSCs), while 3/5 exhibited inhibitory PSCs (IPSCs), suggesting not all neurons possessed excitatory and inhibitory inputs. In contrast, all neurons recorded from cells+SAP grafts exhibited both EPSPs and IPSCs. The frequency and amplitude of EPSCs and IPSCs across "connected" neurons were similar for cells and cells+SAP grafts, with robust and active functions noted (Figure 6G).

Cell Transplants in the Presence of SAP Scaffolds Reduced Cortical Atrophy, an Effect That Was Enhanced by Acute Implantation after Ischemic Insult

Cortical volume was assessed in all animals to determine the benefit of cell ± SAP implants in protecting against secondary degeneration of the host tissue. In a small cohort of animals killed 1week after ET1 injection, the primary insult was evident by the presence of a large necrotic lesion cavity within the sensorimotor cortex (Figure 7E), surrounded by acellular tissue (Figure 7E'), that without intervention resulted in significant secondary degeneration (32.9 ± 2.1% cortical atrophy; Figures 7A and 7F) by 36 weeks. SAP implants alone minimally protected against atrophy of the host tissue (28.3 ± 2.6%; Figures 7A and 7G). By contrast, cell grafts protected the penumbral tissue and significantly reduced atrophy (ET1 + cells, 18.6 ± 1.9%; Figures 7A and 7H), an effect that was greatest in cells+SAP-grafted animals (11.4 ± 1.3% cortical atrophy; Figures 7A and 7I). In support of the graft-induced protection of the host penumbra, a strong correlation (r2 = 0.858) was observed between staircase performance and cortical atrophy (Figure 7B).

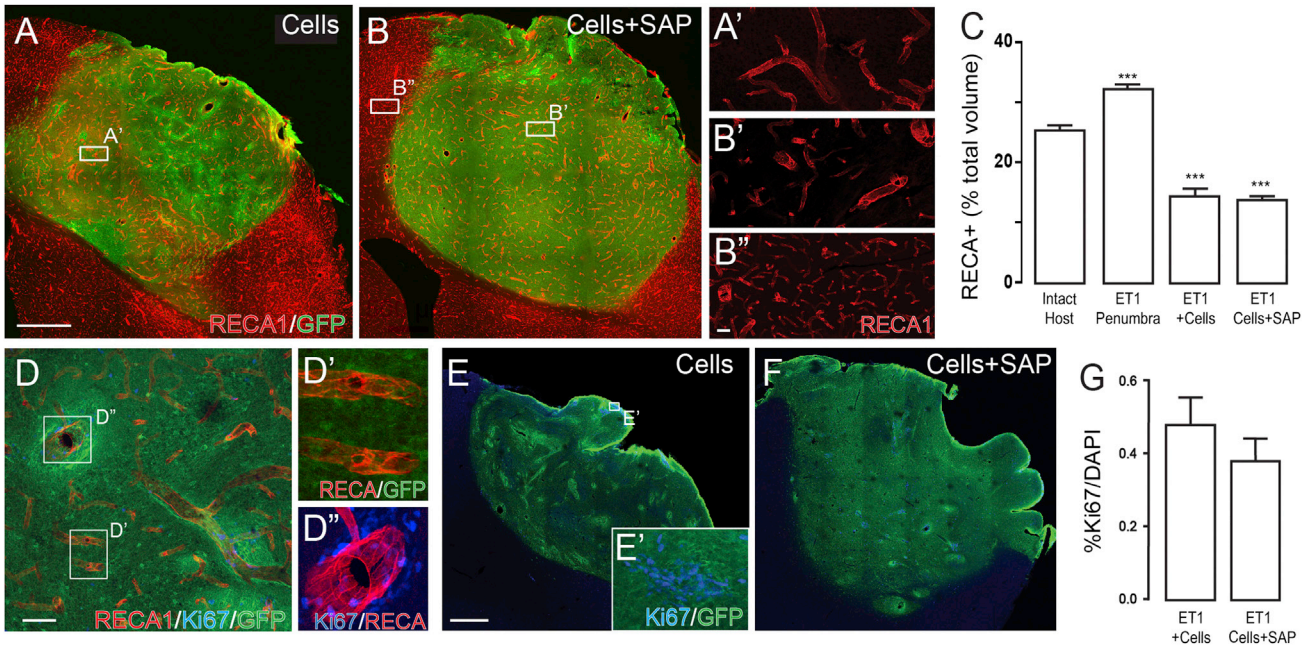

Figure 5. Human ESC-Derived Cortical Progenitor Grafts, in the Presence or Absence of SAP Scaffolds, Are Highly Vascularized by the Host Tissue and Show No Evidence of Tissue Overgrowth

(A–C) Representative images depicting the RECA1$^+$ vascular network within the GFP$^+$ cell graft of an ET-1-lesioned rat in the absence (A) and presence of a SAP scaffold (B). RECA1$^+$ vessels within the graft appeared hypertrophied (A' and B') compared to the host brain (B"). The area covered by RECA1$^+$ staining was significantly reduced within the grafts compared to the intact brain, suggestive of immature vessel development, yet hypervascularization was observed in the adjacent penumbra (C).

(D and D') RECA$^+$ cells within the grafts were GFP$^-$, indicative of host endothelial progenitors vascularizing the grafts (D and D').

(D" and E–G) Representative image of a cell (E) and cells+SAP graft (F) showing the presence of Ki67$^+$ proliferating cells, that were notably few within the grafts (G), and commonly associated with RECA1$^+$ vessels (D"), suggestive of involvement of host-derived vessel formation.

Scale bars, 500 μm (A, B, E, and F) and 50 μm (A', B', B", and D).

While the majority of animals received transplants (cells ± SAP) at 3 weeks post-ET1 lesioning to assess the impact on functional integration and neuroprotection, an additional cohort of animals received implants at 6 days following ET1 administration in an effort to intervene earlier in protection against secondary degeneration and reduce cortical atrophy. Earlier intervention (at 6 days) provided no further protection against atrophy compared to later transplantation (at 3 weeks) for either SAP or cell-grafted animals (Figures 7A, 7G, 7H, 7J, and 7K). However, early implants of cells+SAP significantly reduced atrophy (4.9 ± 0.8%) compared to intervention at 3 weeks (Figures 7A, 7I, and 7L). Note, graft volume and cellular composition did not significantly vary between the two implantation times for either cells or cells+SAP grafts (data not shown).

At 36 weeks after implantation, we quantified groups for the density of cells within the host cortex to assess whether loss of cortical volume correlated with neuronal loss. Within a pre-determined area adjacent to the lesion site (Figures 7D', F', K', and L'), NEUN$^+$ neuronal density remained unchanged in saline and ET1-treated rats (Figure 7C), indicating atrophy was proportionate to cell loss. NEUN density within the host cortex was elevated in cells and cells+SAP-transplanted animals, suggesting that atrophy of the cortex was greater than the proportion of cell loss (Figure 7C).

DISCUSSION

Promoting repair following ischemic stroke will require targeted tissue engineering, including replacement cells, a substratum to support the integration of new cells, protection of the surrounding host, and revascularization of new and old tissue. Here, we report that a tissue-customized self-assembling peptide-based scaffold was capable of interfacing with both replacement neurons generated from human stem cells and residual host tissue, thereby creating a de novo tissue that induced sustained functional recovery in an animal model of focal ischemia.

Numerous biomaterials have been developed to model the native three-dimensional environment of neural tissue, including both natural and synthetic polymers assembled as nanofibers, microspheres, or hydrogels. Such biomaterials have been demonstrated to promote the survival, proliferation, differentiation, and connectivity of neural cells in vitro (see review Rodriguez et al., 2012), yet have been decidedly more difficult to deploy and assess in vivo due to their bulkiness and lack of biocompatibility. Here, we demonstrate the practical utility of a SAP scaffold that post-injection presents IKVAV in a nanofibrous gel, while maintaining a modulus similar to the rat brain, and is capable of supporting cell adhesion and axonal growth in vivo.

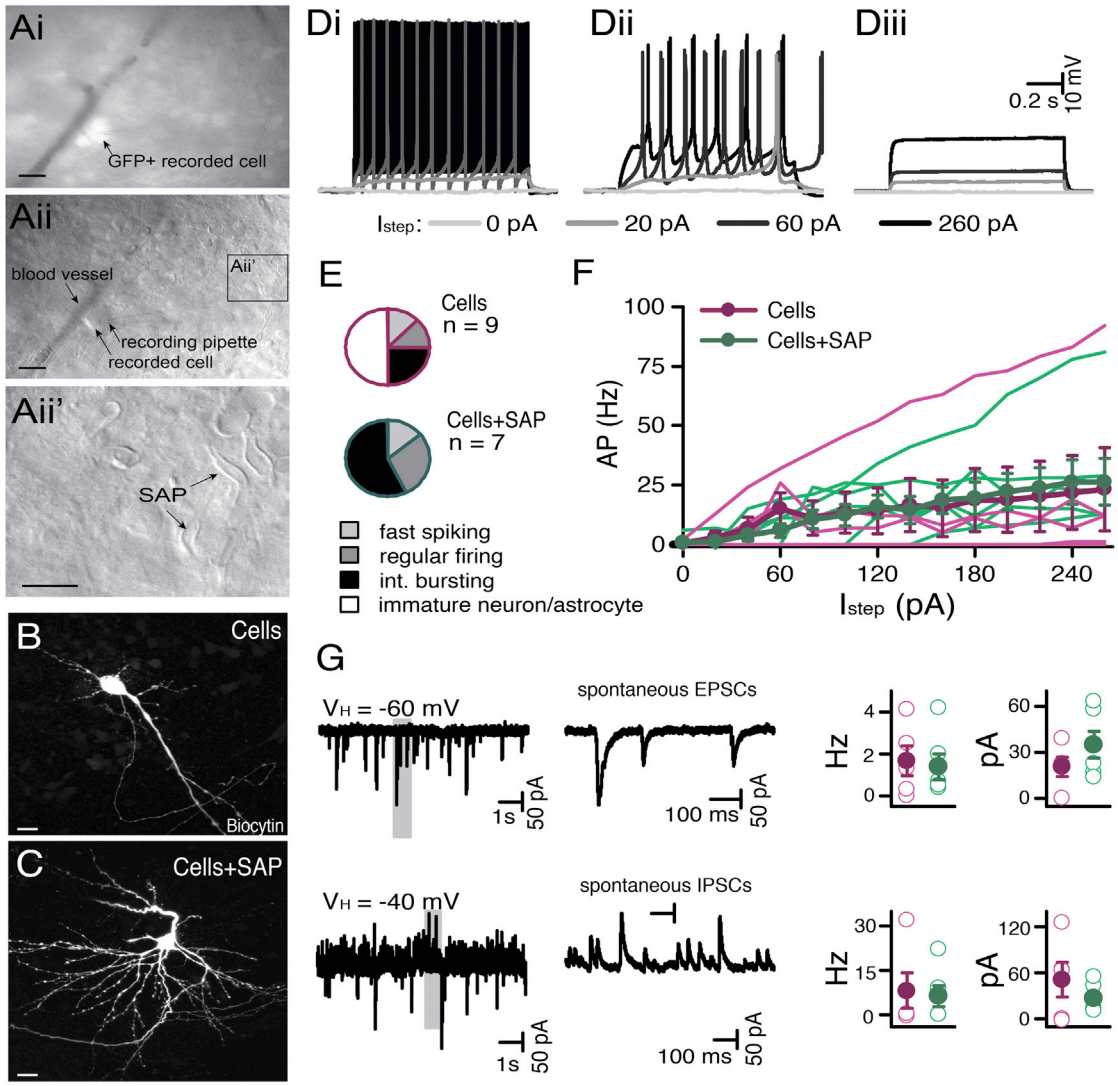

Figure 6. Human ESC-Derived Cortical Progenitors, Implanted in the Presence of SAP Scaffolds into the Ischemic Brain, Exclusively Displayed a Neuronal Phenotype and Enhanced Synaptic Connectivity at 9 Months

(A) Micrographs depicting GFP$^+$ recorded cell within a rodent brain slice and the presence of SAP scaffolds at 36 weeks.

(B and C) Biocytin-filled neuron from cells (B) and cells+SAP graft (C), highlighting their mature neuronal morphology.

(Di–Diii) Depolarizing cells with current injections evoked varying response in GFP positive cells, where fast spiking (Di), intermittent bursting (Dii), and immature neuron/astrocyte-like (Diii) responses were observed.

(E) All cells recorded in the presence of the SAP scaffold were neurons, whereas cells recorded from grafts lacking SAP scaffolds commonly exhibited immature neuronal/astrocyte-like characteristics.

(F) Evoked action potentials (AP) were similar across neurons regardless of the presence of SAP scaffolds, although recorded cells in the absence of SAP tended to exhibit greater variability.

(G) All neurons recorded in the presence of SAP scaffolds exhibited spontaneous excitatory and inhibitory post-synaptic currents (EPSCs and IPSCs, traces from the same neuron). Whereas EPSCs and IPSCs were absent in some neurons patched from cell-alone grafts, indicating comparatively limited synaptic connectivity. The frequency and amplitude of EPSCs and IPSCs across connected neurons were similar across cells and cells+SAP recorded cells, with robust and active function noted.

Scale bars, 20 μm (A–C).

Delivery of the biomaterial directly into the lesion cavity provided an advantage over implantation into the already vulnerable surrounding host penumbral tissue, which could lead to iatrogenic complications. Within the injured brain, these scaffolds formed de novo "bio-bridges" between the lesion cavity, implanted cells, and host tissue. While scaffolds alone showed minimal protection of host tissue and function, advantages of the scaffolding were evident in conjunction with stem cell grafts, resulting in larger, more differentiated transplants than implants of cells alone.

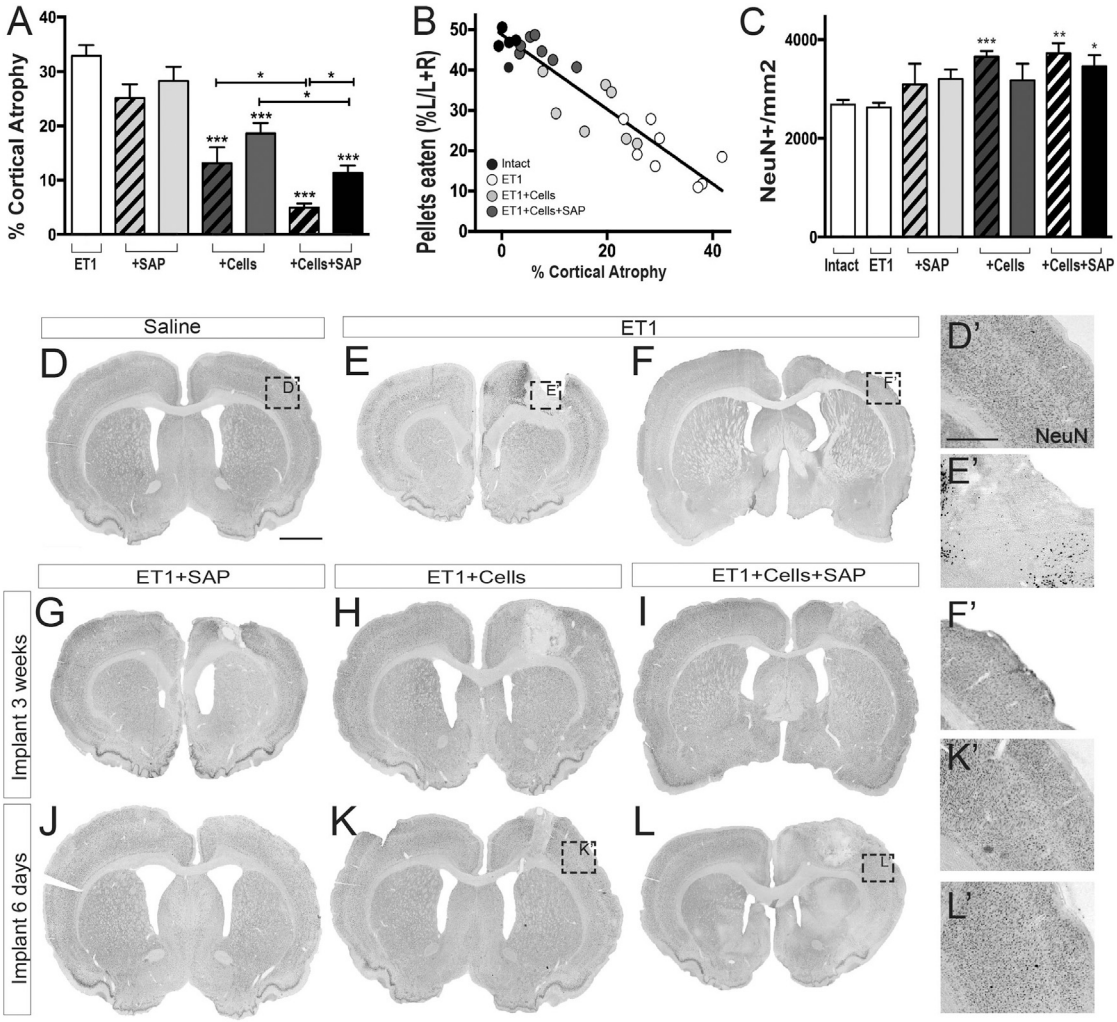

Figure 7. hESC-Derived Cortical Progenitor Grafts in the Presence of SAP Scaffolds Reduce Cortical Atrophy, Improving Motor Function after Focal Ischemia

(A) Comparative assessment of percentage cortical tissue loss across the different treatment groups and of the different times of intervention (i.e., at 3 weeks, open bars versus 6 days, striped bars). Note, earlier intervention significantly reduced atrophy in the presence of cells+SAP.

(B) Regression analyses at 36 weeks highlighted a strong negative correlation between cortical atrophy and motor function, whereby animals displaying the greatest atrophy (ungrafted; ET1, open circles) showed the poorest performance (pellet retrievals) in the staircase test, while cell (light gray)-grafted animals showed reduced atrophy and improved function, that was aided by the presence of scaffolds (cells+SAP, dark gray).

(C) Density of $NEUN^+$ cells within the host cortex, adjacent to the site of injection, showed modest increases in neuronal density in cell-implanted animals, suggestive that the extent of cortical tissue loss exceeded neuronal loss.

(D–L) Representative coronal images of NeuN staining highlighting the gross morphology of the cortex in a saline-injected rat at 36 weeks (D), and following ET-1 injection at 1 week (E), and 36 weeks (F). Note the presence of the lesion cavity at 1 week and progressive cortical collapse and atrophy by 36 weeks. Implantation of SAP scaffolds at 6 days (G) or 3 weeks (J) offered little protection against atrophy, while cell grafts in the absence (H and K) or presence of SAP scaffolds (I and L) visibly protected the host tissue.

(D', E', F', K', L') Higher magnification images from (D–F, K, and L) illustrating NEUN cell density. Scale bars, 2 mm (D–L) and 500 μm (D', E', F', K', and L').

In addition to the structural support provided by the scaffold nanofibrils, which likely contributed to improved graft survival and integration, were the benefits of tissue-specific scaffold presentation of the functional laminin epitope, IKVAV. Previous studies have reported IKVAV, the motif from the a1 chain of the laminin-1 peptide sequence, promotes neuronal cell attachment, migration, differentiation, and neurite outgrowth (Cheng et al., 2013; Silva et al., 2004; Tashiro et al., 1989), including that of hESC-derived neurons (Ma et al., 2008). In support, here, we report enhanced neuronal specification of hESC-derived neural grafts in the presence of the IKVAV scaffold, as well as augmented deep (TBR1) and superficial (BRN2) cortical layer specification of NPCs, necessary for the replacement of neurons lost to the primary insult. Despite the generation of cortical subpopulations and presence of laminin signaling in the present study, no evidence of lamination was observed. This has been

a common issue for cortical transplants into both the intact or infarcted cortex and likely reflects the absence of pial and ventricular surfaces, as well as radial glial cells. Such observations highlight room for further refinement of scaffolds in an effort to recreate such organized structures within the lesion cavity.

A key attribute of the present study was the employment of ubiquitously expressing GFP human ESC-derived NPCs for transplantation, enabling detailed, protracted (9 month) assessment of graft composition and integration into the ischemic brain and in the presence of a biological scaffold. The constitutive GFP reporter line enabled detailed assessment of fiber growth patterns from the graft into the surrounding host tissue. Similar to previous reports of hPSC-derived cortical progenitors into the intact brain (Denham et al., 2012; Espuny-Camacho et al., 2013; Niclis et al., 2017b; Steinbeck et al., 2012), and showing little difference in patterns of innervation between cells and cells+SAP implants, fiber growth closely mimicked the intrinsic projections of the adult brain. Dense GFP innervation was observed most notably within the ipsi- and contralateral cortex, yet axons additionally extended through the external and internal capsule to distal caudal sites, consistent with replacement of lost cortical connections. Further studies will be required to determine the nature of functional synaptic connectivity in these remotely innervated brain regions. However, it is reasonable to speculate synaptic connectivity as a likely outcome, given recent monosynaptic tracing and electron microscopy studies demonstrating this as a property of transplanted neurons generated from pluripotent stem cells (Doerr et al., 2017; Grealish et al., 2015).

Reflective of the morphological differences observed in the hESC-derived grafts in the absence and presence of the scaffold (notably graft size and cortical fate) was graft function. Electrophysiological recordings from cells+SAP-implanted animals revealed all recorded cells were functional neurons and demonstrated a higher degree of synaptic connectivity than grafts of cells alone, as evident by the presence of both inhibitory and excitatory inputs. In support of these findings, cells+SAP-implanted animals showed greater improvements in motor function and/or more rapid restoration of deficits than for animals receiving cell-only implants.

Mechanisms underlying the improvement in graft function remain a key question in cell-based therapy for repair of the ischemic brain. To what extent do transplanted cells provide replacement neurons verses trophism and protection of the host tissue? Observations of improved motor function as early as 8 weeks post-implantation, in both cells and cells+SAP-grafted animals, likely reflect trophism and is supported by the reduction in host cortical atrophy, notably the enhanced protection induced by earlier intervention. Additional functional improvement manifested between 16 and 36 weeks after grafting, particularly in the cells+SAP group. This is a time frame consistent with extensive axonal outgrowth and electrophysiological maturity observed in other grafting studies (Denham et al., 2012; Espuny-Camacho et al., 2013; Niclis et al., 2017b; Steinbeck et al., 2012), and was complemented by correlative increases in graft size and neuronal (including cortical layer specific) differentiation, and likely reflect functional integration of implanted neurons as a contributing therapeutic mechanism. More detailed studies, employing engineered stem cell lines that can be silenced (by expressing light sensitive halorhodopsin or designer receptors exclusively activated by designer drug proteins), that have confirmed functional graft integration in Parkinson's disease (Chen et al., 2016; Steinbeck et al., 2015), will be required to quantitate relative contributions from cell replacement and/or neuroprotection. On balance, it is important to understand the appropriate timing of transplantation after stroke to ensure maximal survival, integration, and function. Unlike previous reports (Darsalia et al., 2011), only in animals receiving cell grafts in the presence of the SAP scaffold was early intervention advantageous, baring no impact on graft composition, but importantly enhancing protection of the penumbra and highlighting the importance of timing as a determinant of outcome for cell-based approaches to ischemic injury.

In summary, we report here long-term survival, integration, and therapeutic efficacy of neural grafts embedded in a self-assembling scaffold matrix after acute implantation into the ischemic cortex. The results show that the use of a readily injectable biomaterial provides significant advantage over cells alone when targeting the hostile environment presented by the stroke-affected tissue and additionally facilitates the survival and maturation of implanted neurons, as well as promotes substantial axonal outgrowth. Although acute neuroprotection appears to be the major contributing mechanism to recovery of motor function, the anatomical patterns of connectivity revealed by GFP^+ fiber outgrowth and the functional maturation of implanted cells suggest that functional replacement of cortical circuitry is an attainable goal as an additional source of therapeutic benefit.

EXPERIMENTAL PROCEDURES

Preparation of Self-Assembling Peptide Scaffolds

A tissue-specific SAP for the brains major extracellular matrix (ECM) protein, laminin, was made using solid phase peptide synthesis (SPPS), as previously described (Rodriguez et al., 2013). In brief, peptide synthesis was achieved by the stepwise deprotection of the N-terminal Fmoc group of the resin-anchored amino acid, followed by a coupling step. Two aspartate residues were incorporated at the N terminus of the peptide to lower the pKa and enable assembly under physiological conditions (pH 7.4). This process of deprotection and coupling of amino acids was repeated until the desired laminin-based epitope was synthesized, aspartate-aspartate-isoleucine-lysine-valine-alanine-valine (DDIKVAV; Figure 1A). Fourier transform infrared (FTIR), circular dichroism (CD) spectroscopy, electron microscopy, and rheology were performed as previously described to verify synthesis, structure, and modulus of the peptide and resultant gel (Rodriguez et al., 2013, 2014). On day of use, Fmoc-SAP powder was dissolved to 20 mg/mL in deionized water and pH corrected to 7.4. At time of implantation, the gel underwent mechanical sheering and was mixed 1:1 with Hank's balanced salt solution (HBSS) or cells.

Differentiation of Human Embryonic Stem Cells

The human ESC line, HES3-ENVY, constitutively expressing GFP under the human β-actin promoter (Costa et al., 2005),was cultured and differentiated using a dual SMAD dorsal forebrain differentiation protocol, as previously described (Denham et al., 2012). After 17 days, neurospheres were either (1) cryopreserved and sectioned for immunohistochemical analysis or (2) dissociated (Accutase, Invitrogen) to provide a single cell suspension (100,000 cells/μL). At the time of implantation, cells were diluted 1:1 in the hydrogel or HBSS media to a final density of 50,000 cells/μL.

Endothelin-1-Induced Ischemia and Cell Transplantation

Animal procedures were conducted in accordance with the Australian National Health and Medical Research Council's published Code of Practice for the Use

of Animals in Research, and the Florey Neuroscience Institute animal ethics committee approved experiments. Surgeries were performed on athymic (CBH^{rnu}) nude rats under general anesthetic (2% isoflurane). Focal ischemia was modeled in 109 rats by unilateral injections (2 × 0.5 μL) of the vasoconstrictor endothelin-1 (400 pmol/μL, AusPep, Australia) into the right sensorimotor cortex (0.5 and 2.0 mm anterior, 2.5 mm lateral relative to bregma, and 1.5 mm below the dura). 12 additional rats were used as unlesioned controls, receiving saline injections. At 6 days or 3 weeks after lesioning, animals received two intracortical injections (1 μL each) of hESC-derived cortical progenitor and/or SAP gels into the lesion site (above co-ordinates). Final concentration of implanted SAP gels was 10 mg/mL and total number of cells 100,000/rat.

Behavior

The modified staircase test (Winkler et al., 1999) was commenced 1 week after ET1 lesioning (T = 0 weeks, pre-graft) and repeated at 4, 8, 16, 24, and 36 weeks following implants. Rats were food-restricted for the 7 day test duration, placed in the staircase apparatus daily (Campden Instruments, UK), and pellets retrieved and eaten recorded over 20 min. Impaired (left) paw retrievals were expressed as a percentage of total (%L/L + R) and averaged over the last 3 test days. At T = 0 weeks, only animals capable of retrieving a minimum of 20 pellets with the unimpaired forepaw were included in the study, and only animals showing ≤33% of pellet retrievals with the impaired paw were deemed to have sufficient lesions of the motor cortex to warrant inclusion. Rotarod performance test was conducted in rats at 36 weeks following cells ± SAP implantation. Animals were placed on a horizontal, suspended, accelerating rotating rod (3–40 rpm) and the latency to fall (max 5 min) recorded, and each received three consecutive trials. Cylinder test was performed at 36 weeks post implantation. Animals were placed in a glass cylinder (20 cm diameter), and two observers recorded weight-bearing forepaw wall contacts (max 20 per animal, expressed as a percentage of impaired touches/total). Stepping test was performed as described previously (Olsson et al., 1995). Rats were restrained by the experimenter, allowing them to make unilateral forepaw weight-bearing contact with the bench, and were assessed for their ability to make stepping adjustments with the paw when moved laterally over a 1 m distance. Number of steps made by weight-bearing forepaws was recorded in both the forehand and backhand direction, with testing repeated 3 times/day over 5 days.

Tissue Processing and Histology

The majority of animals were killed by an overdose of sodium pentobarbitone (100 mg/kg) and processed for immunohistochemistry, as previously described (Denham et al., 2012). Primary antibodies: rabbit anti-5HT (1:1,000, Immunostar), rabbit anti-BRN2 (1:200, Santa Cruz), goat anti-choline acetyltransferase (1:100, Millipore), goat anti-doublecortin (1:400; Santa Cruz), rabbit anti-GFAP (1:200, Dako), chicken anti-GFP (1:1,000; Abcam), rabbit anti-GFP (1:20,000; Abcam), mouse rabbit anti-Ki67 (1:1,000, Novocastra), mouse anti-NEUN (1:100; R&D Systems), rabbit anti-OLIG2 (1:200, Millipore), rabbit anti-OTX2 (1:4,000, Millipore), mouse anti-PAX6 (1:50, Developmental Studies Hybridoma Bank [DSHB]), anti-rat endothelial cell antigen-1 (RECA-1, 1:500, Serotec), mouse anti-RIP (1:5,000, Millipore), goat anti-SOX2 (1:200; R&D), TBR1 (1:1,000, Millipore), tyrosine hydroxylase (TH, 1:800, Pel-Freez), mouse anti-vesicular glutamate transporter 1 (vGLUT, 1:200, Millipore, MAB5504).

Assessment of Host and Graft Tissue

Atrophy and neuronal cell loss within the host cortex were quantified in control and ET1-lesioned rats, immuno-labeled with NEUN, at 36 weeks after cell ± SAP implants. Ipsilateral cortical atrophy was quantified from a 1:12 series, spanning 2.7 mm rostral to 2.1 mm caudal to bregma (five sections, Figures S1, related to 7), and expressed as a percentage of control (saline injected) cortex. Volume was calculated from the sum of areas, section thickness, and interval, according to Cavalieri's principle.

NEUN cell loss was estimated from the two sections (0.8 and 1.7 mm rostral to bregma) ventro-lateral to the infarct core (Figures 7D–7F, 7K, and 7L, see boxed insets). Stereological counts were made in the delineated area (1.5 × 1.5 mm) at regular pre-determined intervals (200 × 200 μm), within a counting frame (40 × 40 μm), and guard zones set at 1 μm, as previously described (Parish et al., 2001).

PSC grafts were identified by GFP-labeling with volumetric assessments, cell counts (DAPI, NEUN, BRN2, and TBR1), and densities performed stereologically. Counts were made at the following pre-determined intervals (DAPI: 500 × 500 μm; NEUN: 400 × 400 μm; and TBR1 and BRN2: 280 × 280 μm) using counting frames of known areas (DAPI: 10 × 10 μm; NEUN: 20 × 20 μm; and TBR1 and BRN2: 30 × 30 μm). For all counts, the co-efficient of error (CE) and co-efficient of variance (CV) were calculated as estimates of precision and values of less than 0.1 were accepted (West et al., 1991).

Graft innervation of host tissue was assessed in the motor cortex adjacent to the graft core (Figures 4B and 4Bi) and distal targets, the ipsilateral and contralateral entorhinal cortex (Figures 4B, 4Biii, and 4Biv). Leica LAS Image Analysis Software was used to estimate fiber density.

$RECA\text{-}1^+$ vessel density was estimated from three sections/graft, with five sites (20× magnification) randomly sampled per section, as well as five sites within the host tissue, yet within 500 μm of the graft edge (identified by the GFP^+/GFP^- border), and indicative of the surrounding penumbra. Host vessel density was additionally assessed from the contralateral hemisphere of the saline-injected rats. Vessel density was expressed as the percentage total area covered by RECA-1 staining, averaged across the sampling sites. The diameter of 75 $RECA\text{-}1^+$ vessel, randomly sampled from the three sections per graft, as well as in the surrounding host tissue, was quantified for each brain.

Electrophysiology

Coronal forebrain slices were prepared from cells and cells+SAP-implanted rats (n = 3/group) and whole-cell electrophysiology performed as previously described (Denham et al., 2012; Niclis et al., 2017a). Biocytin (0.5%) was added to the recording pipette to fill neurons after recordings, enabling confirmation of graft origin (GFP^+ cytochemistry) and visualization of cell morphology (Figures 6B and 6C).

Statistical Analysis

Tests performed to identify significant changes between animal groups included: repeated-measures ANOVA, one-way ANOVAs with Tukey post hoc, and Student's t tests. Data represent mean ± SEM, with statistical significant set at a level of 0.05, $^*p < 0.05$, $^{**}p < 0.01$, and $^{***}p < 0.001$.

SUPPLEMENTAL INFORMATION

Supplemental Information includes three figures and can be found with this article online at http://dx.doi.org/10.1016/j.celrep.2017.07.069.

AUTHOR CONTRIBUTIONS

F.A.S.: collection and assembly of data, manuscript preparation, and final approval of manuscript. T.Y.W.: collection and assembly of data and final approval of manuscript. J.C.N.: collection and assembly of data, manuscript preparation, and final approval of manuscript. K.F.B.: collection and assembly of data and final approval of manuscript. J.A.K.: collection and assembly of data and final approval of manuscript. H.G.: collection and assembly of data and final approval of manuscript. S.M.: collection and assembly of data and final approval of manuscript. R.J.W.: supply of reagents, assembly of data, and final approval of manuscript. D.R.N.: financial support, collection and assembly of data, interpretation of findings, and final approval of manuscript. L.H.T.: financial support, collection and assembly of data, interpretation of findings, manuscript preparation, and final approval of manuscript. C.L.P.: financial support, collection and assembly of data, interpretation of findings, manuscript preparation, and final approval of manuscript.

ACKNOWLEDGMENTS

This research was supported by funding from the National Health and Medical Research Council Australia (APP1122974), the Australian Research Council (130103131), and CASS Foundation, Australia. The Florey Institute of Neuroscience and Mental Health acknowledges support from the Victorian Government's Operational Infrastructure Support grant. K.F.B. was supported by a Natural Sciences and Engineering Research Council of Canada Postgraduate

Scholarship Doctoral award; D.R.N. was supported by an NHMRC Career Development Fellowship; and C.L.P. was supported by a Senior Medical Research Fellowship provided by the Viertel Charitable Foundation, Australia. Access to the facilities of the Centre for Advanced Microscopy, with funding through the Australian Microscopy and Microanalysis Research Facility, is gratefully acknowledged. The authors thank Ms. Mong Tien for her technical assistance with tissue processing and histochemistry.

Received: February 23, 2017
Revised: June 7, 2017
Accepted: July 24, 2017
Published: August 22, 2017

REFERENCES

Barker, R.A., Barrett, J., Mason, S.L., and Björklund, A. (2013). Fetal dopaminergic transplantation trials and the future of neural grafting in Parkinson's disease. Lancet Neurol. *12*, 84–91.

Bible, E., Chau, D.Y., Alexander, M.R., Price, J., Shakesheff, K.M., and Modo, M. (2009). The support of neural stem cells transplanted into stroke-induced brain cavities by PLGA particles. Biomaterials *30*, 2985–2994.

Bible, E., Qutachi, O., Chau, D.Y., Alexander, M.R., Shakesheff, K.M., and Modo, M. (2012). Neo-vascularization of the stroke cavity by implantation of human neural stem cells on VEGF-releasing PLGA microparticles. Biomaterials *33*, 7435–7446.

Cao, W., and Li, P. (2015). Effectiveness and safety of autologous bone marrow stromal cells transplantation after ischemic stroke: a meta-analysis. Med. Sci. Monit. *21*, 2190–2195.

Casper, D., Finkelstein, E., Goldstein, I.M., Palencia, D., Yunger, Y., and Pidel, A. (2003). Dopaminergic neurons associate with blood vessels in neural transplants. Exp. Neurol. *184*, 785–793.

Chambers, S.M., Fasano, C.A., Papapetrou, E.P., Tomishima, M., Sadelain, M., and Studer, L. (2009). Highly efficient neural conversion of human ES and iPS cells by dual inhibition of SMAD signaling. Nat. Biotechnol. *27*, 275–280.

Chen, Y., Xiong, M., Dong, Y., Haberman, A., Cao, J., Liu, H., Zhou, W., and Zhang, S.C. (2016). Chemical control of grafted human PSC-derived neurons in a mouse model of Parkinson's disease. Cell Stem Cell *18*, 817–826.

Cheng, T.Y., Chen, M.H., Chang, W.H., Huang, M.Y., and Wang, T.W. (2013). Neural stem cells encapsulated in a functionalized self-assembling peptide hydrogel for brain tissue engineering. Biomaterials *34*, 2005–2016.

Costa, M., Dottori, M., Ng, E., Hawes, S.M., Sourris, K., Jamshidi, P., Pera, M.F., Elefanty, A.G., and Stanley, E.G. (2005). The hESC line Envy expresses high levels of GFP in all differentiated progeny. Nat. Methods *2*, 259–260.

Daadi, M.M., Maag, A.L., and Steinberg, G.K. (2008). Adherent self-renewable human embryonic stem cell-derived neural stem cell line: functional engraftment in experimental stroke model. PLoS ONE *3*, e1644.

Darsalia, V., Allison, S.J., Cusulin, C., Monni, E., Kuzdas, D., Kallur, T., Lindvall, O., and Kokaia, Z. (2011). Cell number and timing of transplantation determine survival of human neural stem cell grafts in stroke-damaged rat brain. J. Cereb. Blood Flow Metab. *31*, 235–242.

Denham, M., Parish, C.L., Leaw, B., Wright, J., Reid, C.A., Petrou, S., Dottori, M., and Thompson, L.H. (2012). Neurons derived from human embryonic stem cells extend long-distance axonal projections through growth along host white matter tracts after intra-cerebral transplantation. Front. Cell. Neurosci. *6*, 11.

Doerr, J., Schwarz, M.K., Wiedermann, D., Leinhaas, A., Jakobs, A., Schloen, F., Schwarz, I., Diedenhofen, M., Braun, N.C., Koch, P., et al. (2017). Whole-brain 3D mapping of human neural transplant innervation. Nat. Commun. *8*, 14162.

Elias, P.Z., and Spector, M. (2012). Implantation of a collagen scaffold seeded with adult rat hippocampal progenitors in a rat model of penetrating brain injury. J. Neurosci. Methods *209*, 199–211.

Ellis-Behnke, R.G., Liang, Y.X., You, S.W., Tay, D.K., Zhang, S., So, K.F., and Schneider, G.E. (2006). Nano neuro knitting: peptide nanofiber scaffold for brain repair and axon regeneration with functional return of vision. Proc. Natl. Acad. Sci. USA *103*, 5054–5059.

Espuny-Camacho, I., Michelsen, K.A., Gall, D., Linaro, D., Hasche, A., Bonnefont, J., Bali, C., Orduz, D., Bilheu, A., Herpoel, A., et al. (2013). Pyramidal neurons derived from human pluripotent stem cells integrate efficiently into mouse brain circuits in vivo. Neuron *77*, 440–456.

Gomi, M., Takagi, Y., Morizane, A., Doi, D., Nishimura, M., Miyamoto, S., and Takahashi, J. (2012). Functional recovery of the murine brain ischemia model using human induced pluripotent stem cell-derived telencephalic progenitors. Brain Res. *1459*, 52–60.

Grealish, S., Heuer, A., Cardoso, T., Kirkeby, A., Jönsson, M., Johansson, J., Björklund, A., Jakobsson, J., and Parmar, M. (2015). Monosynaptic tracing using modified rabies virus reveals early and extensive circuit integration of human embryonic stem cell-derived neurons. Stem Cell Reports *4*, 975–983.

Guo, J., Leung, K.K., Su, H., Yuan, Q., Wang, L., Chu, T.H., Zhang, W., Pu, J.K., Ng, G.K., Wong, W.M., et al. (2009). Self-assembling peptide nanofiber scaffold promotes the reconstruction of acutely injured brain. Nanomedicine (Lond.) *5*, 345–351.

Jendelová, P., Kubinová, Š., Sandvig, I., Erceg, S., Sandvig, A., and Syková, E. (2016). Current developments in cell- and biomaterial-based approaches for stroke repair. Expert Opin. Biol. Ther. *16*, 43–56.

Jensen, M.B., Yan, H., Krishnaney-Davison, R., Al Sawaf, A., and Zhang, S.C. (2013). Survival and differentiation of transplanted neural stem cells derived from human induced pluripotent stem cells in a rat stroke model. J. Stroke Cerebrovasc. Dis. *22*, 304–308.

Jiang, M., Lv, L., Ji, H., Yang, X., Zhu, W., Cai, L., Gu, X., Chai, C., Huang, S., Sun, J., and Dong, Q. (2011). Induction of pluripotent stem cells transplantation therapy for ischemic stroke. Mol. Cell. Biochem. *354*, 67–75.

Jin, K., Mao, X., Xie, L., Galvan, V., Lai, B., Wang, Y., Gorostiza, O., Wang, X., and Greenberg, D.A. (2010). Transplantation of human neural precursor cells in Matrigel scaffolding improves outcome from focal cerebral ischemia after delayed postischemic treatment in rats. J. Cereb. Blood Flow Metab. *30*, 534–544.

Liang, Y., Walczak, P., and Bulte, J.W. (2013). The survival of engrafted neural stem cells within hyaluronic acid hydrogels. Biomaterials *34*, 5521–5529.

Lindvall, O., and Kokaia, Z. (2011). Stem cell research in stroke: how far from the clinic? Stroke *42*, 2369–2375.

Ma, W., Tavakoli, T., Derby, E., Serebryakova, Y., Rao, M.S., and Mattson, M.P. (2008). Cell-extracellular matrix interactions regulate neural differentiation of human embryonic stem cells. BMC Dev. Biol. *8*, 90.

Matson, J.B., Zha, R.H., and Stupp, S.I. (2011). Peptide self-assembly for crafting functional biological materials. Curr. Opin. Solid State Mater. Sci. *15*, 225–235.

Niclis, J.C., Gantner, C.W., Alsanie, W.F., McDougall, S.J., Bye, C.R., Elefanty, A.G., Stanley, E.G., Haynes, J.M., Pouton, C.W., Thompson, L.H., and Parish, C.L. (2017a). Efficiently specified ventral midbrain dopamine neurons from human pluripotent stem cells under xeno-free conditions restore motor deficits in Parkinsonian rodents. Stem Cells Transl. Med. *6*, 937–948.

Niclis, J.C., Turner, C., Durnall, J., McDougal, S., Kauhausen, J.A., Leaw, B., Dottori, M., Parish, C.L., and Thompson, L.H. (2017b). Long-distance axonal growth and protracted functional maturation of neurons derived from human induced pluripotent stem cells after intracerebral transplantation. Stem Cells Transl. Med. *6*, 1547–1556.

Oki, K., Tatarishvili, J., Wood, J., Koch, P., Wattananit, S., Mine, Y., Monni, E., Tornero, D., Ahlenius, H., Ladewig, J., et al. (2012). Human-induced pluripotent stem cells form functional neurons and improve recovery after grafting in stroke-damaged brain. Stem Cells *30*, 1120–1133.

Olsson, M., Nikkhah, G., Bentlage, C., and Björklund, A. (1995). Forelimb akinesia in the rat Parkinson model: differential effects of dopamine agonists and nigral transplants as assessed by a new stepping test. J. Neurosci. *15*, 3863–3875.

Parish, C.L., Finkelstein, D.I., Drago, J., Borrelli, E., and Horne, M.K. (2001). The role of dopamine receptors in regulating the size of axonal arbors. J. Neurosci. *21*, 5147–5157.

Park, K.I., Teng, Y.D., and Snyder, E.Y. (2002). The injured brain interacts reciprocally with neural stem cells supported by scaffolds to reconstitute lost tissue. Nat. Biotechnol. *20*, 1111–1117.

Qin, J., Gong, G., Sun, S., Qi, J., Zhang, H., Wang, Y., Wang, N., Wang, Q.M., Ji, Y., Gao, Y., et al. (2013). Functional recovery after transplantation of induced pluripotent stem cells in a rat hemorrhagic stroke model. Neurosci. Lett. *554*, 70–75.

Rodriguez, A.L., Nisbet, D.R., and Parish, C.L. (2012). Stem cells and biomaterials for repair of the damaged central nervous system. In Stem Cells and Cancer Stem Cells: Therapeutic Applications in Disease and Injury, M.A. Hayat, ed. (Springer Company), pp. 97–111.

Rodriguez, A.L., Parish, C.L., Nisbet, D.R., and Williams, R.J. (2013). Tuning the amino acid sequence of minimalist peptides to present biological signals via charge neutralised self assembly. Soft Matter *9*, 3915–3919.

Rodriguez, A.L., Wang, T.Y., Bruggeman, K.F., Horgan, C.C., Li, R., Williams, R.J., Parish, C.L., and Nisbet, D.R. (2014). In vivo assessment of grafted cortical neural progenitor cells and host response to functionalized self-assembling peptide hydrogels and the implications for tissue repair. J. Mater. Chem. B Mater. Biol. Med. *2*, 7771–7778.

Sahab Negah, S., Khaksar, Z., Aligholi, H., Mohammad Sadeghi, S., Modarres Mousavi, S.M., Kazemi, H., Jahanbazi Jahan-Abad, A., and Gorji, A. (2016). Enhancement of neural stem cell survival, proliferation, migration, and differentiation in a novel self-assembly peptide nanofibber scaffold. Mol. Neurobiol. Published online November 23, 2016. http://dx.doi.org/10.1007/s12035-016-0295-3.

Shi, Y., Kirwan, P., Smith, J., Robinson, H.P., and Livesey, F.J. (2012). Human cerebral cortex development from pluripotent stem cells to functional excitatory synapses. Nat. Neurosci. *15*, 477–486, S471.

Silva, G.A., Czeisler, C., Niece, K.L., Beniash, E., Harrington, D.A., Kessler, J.A., and Stupp, S.I. (2004). Selective differentiation of neural progenitor cells by high-epitope density nanofibers. Science *303*, 1352–1355.

Steinbeck, J.A., Koch, P., Derouiche, A., and Brüstle, O. (2012). Human embryonic stem cell-derived neurons establish region-specific, long-range projections in the adult brain. Cell. Mol. Life Sci. *69*, 461–470.

Steinbeck, J.A., Choi, S.J., Mrejeru, A., Ganat, Y., Deisseroth, K., Sulzer, D., Mosharov, E.V., and Studer, L. (2015). Optogenetics enables functional analysis of human embryonic stem cell-derived grafts in a Parkinson's disease model. Nat. Biotechnol. *33*, 204–209.

Tashiro, K., Sephel, G.C., Weeks, B., Sasaki, M., Martin, G.R., Kleinman, H.K., and Yamada, Y. (1989). A synthetic peptide containing the IKVAV sequence from the A chain of laminin mediates cell attachment, migration, and neurite outgrowth. J. Biol. Chem. *264*, 16174–16182.

Tatarishvili, J., Oki, K., Monni, E., Koch, P., Memanishvili, T., Buga, A.M., Verma, V., Popa-Wagner, A., Brüstle, O., Lindvall, O., and Kokaia, Z. (2014). Human induced pluripotent stem cells improve recovery in stroke-injured aged rats. Restor. Neurol. Neurosci. *32*, 547–558.

Thompson, L., and Björklund, A. (2012). Survival, differentiation, and connectivity of ventral mesencephalic dopamine neurons following transplantation. Prog. Brain Res. *200*, 61–95.

Tornero, D., Wattananit, S., Grønning Madsen, M., Koch, P., Wood, J., Tatarishvili, J., Mine, Y., Ge, R., Monni, E., Devaraju, K., et al. (2013). Human induced pluripotent stem cell-derived cortical neurons integrate in stroke-injured cortex and improve functional recovery. Brain *136*, 3561–3577.

West, M.J., Slomianka, L., and Gundersen, H.J. (1991). Unbiased stereological estimation of the total number of neurons in the subdivisions of the rat hippocampus using the optical fractionator. Anat. Rec. *231*, 482–497.

Winkler, C., Bentlage, C., Nikkhah, G., Samii, M., and Björklund, A. (1999). Intranigral transplants of GABA-rich striatal tissue induce behavioral recovery in the rat Parkinson model and promote the effects obtained by intrastriatal dopaminergic transplants. Exp. Neurol. *155*, 165–186.

Yu, H., Cao, B., Feng, M., Zhou, Q., Sun, X., Wu, S., Jin, S., Liu, H., and Lianhong, J. (2010). Combinated transplantation of neural stem cells and collagen type I promote functional recovery after cerebral ischemia in rats. Anat. Rec. (Hoboken) *293*, 911–917.

Zhong, J., Chan, A., Morad, L., Kornblum, H.I., Fan, G., and Carmichael, S.T. (2010). Hydrogel matrix to support stem cell survival after brain transplantation in stroke. Neurorehabil. Neural Repair *24*, 636–644.